The Moist Boundary Layer with a Higher Order Turbulence Closure Model

STEPHEN D. BURK[1]

National Severe Storms Laboratory, NOAA, Norman, Okla. 73069

(Manuscript received 2 September 1976, in revised form 14 December 1976)

ABSTRACT

A one-dimensional higher order turbulence closure model is used to investigate moisture structure within the diurnally varying planetary boundary layer. The diurnal character of the moist boundary layer as a whole and a variety of micrometeorological features are examined in a series of experiments having differing lower boundary conditions on the moisture field. In one case, midafternoon surface evaporation and turbulent moisture transfer to higher levels act as competing processes in determining low-level moisture content. A double wave in low-level daily specific humidity results (specific humidity minima in early morning and midafternoon). In another experiment, a moisture inversion develops when there is a strong nocturnal moisture flux to the surface such as occurs with dew formation.

A simple, analytic method of calculating the moist layer's growth rate is compared with the numerical results. The analytic method provides good flux estimates when the shoulder in the specific humidity profiles (where the moisture lapse first sharply deviates from its mixed-layer value) is treated as being the top of the moist boundary layer.

The specified initial moisture distribution has a considerable lapse above 0.5 km. However, during the afternoon a well-mixed moist layer develops despite dry air entrainment above and surface moisture influx from below. This suggests that rapid growth into a dry environment cannot explain the coincidence of strong moisture lapses with thermally well-mixed regions.

1. Introduction

Both structure and growth of the heated planetary boundary layer (PBL) has been studied in analytical and numerical experiments (Lilly, 1968; Tennekes, 1973; Carson, 1973; Stull, 1973; Deardorff, 1974a,b; Mahrt and Lenschow, 1976). The primary parameters governing the growth rate and penetration depth of the dry thermal boundary layer were elucidated, including detailed features such as entrainment through the capping inversion. However, the structure and temporal behavior of the moist boundary layer has not received comparable attention. Certainly this cannot be due to a lack of importance because the moisture structure in the PBL exerts a profound influence on the dynamic, thermodynamic and radiative transfer properties of our atmosphere. Instead, belief that the nature of the moist layer might readily be deduced from a thorough knowledge of the thermal boundary layer has contributed to this neglect. In many instances this belief is justified. For example, the universal functions for heat and moisture derived from similarity theory generally are equated to each other in the surface boundary layer. Analyzing extensive tower and rawinsonde data taken near Oklahoma City, Schaefer (1976) finds that when the atmosphere above the surface boundary layer is neutrally stratified, the mixing ratio tends to be nearly constant with height. He also shows that the depths of the moist and thermal layers are closely correlated. Wangara data (Clark *et al.*, 1971) yield a similar correlation between moist and thermal structure in the heated PBL when considering cases with no frontal systems within 500 km of the experimental site (Melgarejo and Deardorff, 1974).

Nevertheless, one does find situations in which no well-mixed moist layer exists despite the presence of a thermally well-mixed boundary layer. Mahrt's results (1976) frequently show the absence of a well-mixed moist layer in the National Hail Research Experiment data from the high plains of northeast Colorado and southwest Nebraska. Mahrt proposes that mechanisms such as differential moisture advection and dry air entrainment into the growing convective layer may be responsible for the substantial moisture lapses which he finds within a thermally well-mixed PBL. Although a good correlation between thermal lapse and hydrolapse exists at neutral stratification in Schaefer's results, the data exhibit large scatter for other stratifications. Thus, it is apparent that the moist boundary layer, both more interesting and more complex than generally perceived, deserves closer scrutiny.

Here I investigate the temporal behavior of moisture stratification within the diurnally varying PBL by means of a higher order turbulence closure model similar to that developed by Mellor (1973) and Mellor and Yamada (1974). In this model, the closure assumptions

[1] Present affiliation: Naval Experimental Prediction Research Facility, Monterey, Calif. 93940.

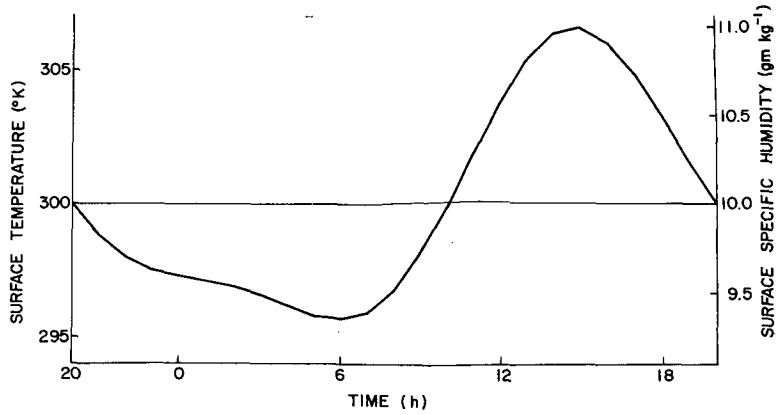

FIG. 1. Specified diurnal wave of surface temperature and surface specific humidity.

are introduced into the dynamic equations for the second turbulent moments. Turbulence closure models (often called ensemble mean closure models) have achieved considerable maturity and have demonstrated a capacity for dealing with a wide range of fluid dynamical problems (Donaldson, 1973; Lumley and Khajeh-Nouri, 1974; Lewellen *et al.*, 1973; Launder *et al.*, 1975).

Simulations of moist layer evolution presented here range from a moist surface with peak evaporation coincident with maximum surface temperature to a dry surface with no moisture flux. A considerable initial moisture lapse is assumed so that the boundary layer's growth into a relatively dry environment may be examined. Although the one-dimensional model rules out inclusion of differential moisture advection, it can assess the effectiveness of surface evaporation and dry air entrainment in maintaining the initial moisture lapse as the PBL undergoes its diurnal cycle.

Also the model provides insight into micrometeorological processes influencing the near-surface moisture distribution. The frequent appearance of a double wave in the daily specific humidity profile measured above about 1 m is well known (Geiger, 1965). The principal minimum in specific humidity occurs near the time of surface temperature minimum, with a secondary minimum at midafternoon. Schaefer (1976) finds this double wave feature present not only in the surface boundary layer realm of micrometeorological concern, but also in his tower data at 444 m. When there is dew formation a strong, near-surface moisture inversion often is present. These features are also prominent in our results and we examine the competing processes which produce them.

2. The model

The model uses the shallow convection Boussinesq equations. Mellor and Yamada (1974) present subsets of their turbulence closure model ranging in complexity from a (Level 4) version in which simultaneous solution of partial differential equations for all turbulent moments are required to one (Level 1) whose equations are reduced to an algebraic set. The level of complexity is reduced by systematic neglect of terms based upon their degree of isotropy. Here use is made of the Level 3 version in which certain of the diffusion and tendency terms were neglected in the turbulent moment equations. For a dry PBL, this model requires solving partial differential equations for the turbulent kinetic energy $\frac{1}{2}q^2$ and potential temperature variance $\overline{\theta^2}$, plus differential equations for the mean variables. Algebraic equations apply for the remaining turbulent moments.

Yamada and Mellor (1975) use the Level 3 version to simulate data from the Wangara experiment. However, they select a less complex (Level 2) subset of purely algebraic equations for computing moisture related fluxes. Since these are the terms of prime concern here, this treatment is also at Level 3 in moisture. This requires solution of partial differential equations for the temperature-moisture covariance $\overline{\theta_v r}$ and the specific humidity variance $\overline{r^2}$.

Subject to specified initial and boundary conditions, numerical solution is sought for the equations of motion, the continuity equation, the thermodynamic equation and the moisture conservation equation. Solution yields the temporal and spatial variation of mean horizontal wind components (U and V), mean virtual potential temperature Θ_v and mean specific humidity R. In a Boussinesq, one-dimensional boundary layer model with flat terrain $\partial/\partial x=\partial/\partial y=0$ and the continuity equation requires that the mean vertical velocity W be zero everywhere.

a. Initial and boundary conditions

Above the lowest 100 m, the finite-difference grid has a uniform spacing ΔZ of 50 m with the grid top at 2500 m. Finer resolution is used in the first 100 m, with grid points at 0.1, 5, 10, 25, 50, 75 and 100 m. Logarithmic (law of the wall) relationships relate surface values of wind, temperature and humidity to their values at the first grid point above the surface. The virtual potential

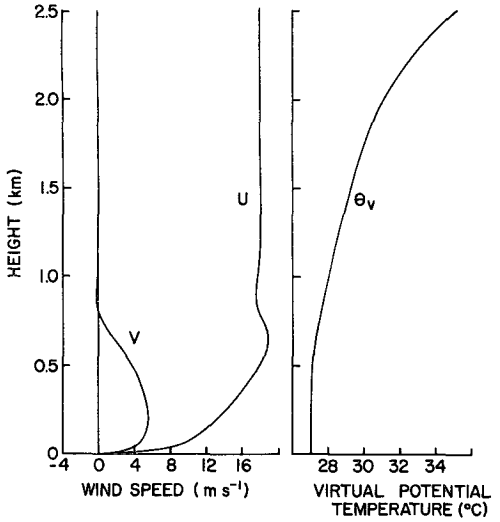

FIG. 2. Initial distributions of wind and temperature.

temperature at roughness height $Z_0(=1$ cm) has the biharmonic variation shown in Fig. 1 (Kuo, 1968), and the "no-slip" ($U=V=0$) boundary condition is used for the wind at Z_0. At the upper boundary, the turbulent fluxes and mean wind shears are assumed as zero, while the lapses of R and Θ_v are held constant. The geostrophic wind is taken as constant with height and time, having the value $U_g=18$ m s^{-1} and $V_g=0$. The Coriolis parameter is fixed at 10^{-4} s^{-1}, which corresponds to about 43°N and gives an inertial period of 17.5 h.

Initial distributions of U, V and Θ_v are shown in Fig. 2. These U and V profiles were obtained by integrating (without thermal forcing) until a quasi-steady-state was attained. The boundary and initial conditions on specific humidity are discussed as each model experiment is reviewed. As with Mellor and Yamada (1974) and Donaldson (1973), the model itself generates initial values of the turbulent moments. This is done here by integrating the system of equations forward using estimated initial values of the turbulent moments. This procedure permits turbulent moments and mean variables to mutually adjust to each other. Results are insensitive both to the initial estimated values of the turbulent moments and also to the length of the adjustment period provided it is 1 h or more.

Initial conditions simulate early evening (2000 LT). Of course, in such a diagnostic model assignment of local time is somewhat arbitrary and so is guided by the chosen surface temperature wave (Fig. 1).

The finite-difference algorithm presented by Yamada and Mellor was found to be numerically unstable under certain conditions. The source of difficulty and a method of correcting it are outlined in the Appendix.

3. Model experiments

a. Specified surface specific humidity

Consider a case in which the lower boundary condition on the moisture distribution requires the surface specific humidity R_s to vary in phase with the surface temperature wave. The amplitude of this humidity cycle is shown in Fig. 1. Measurements of the partial pressure of water vapor show that this type of surface specific humidity variation is rather typical of the lowest several centimeters in temperature climates (Geiger, 1965).

Evolution of the moisture configuration during the first 24 h of integration is displayed in Fig. 3. The

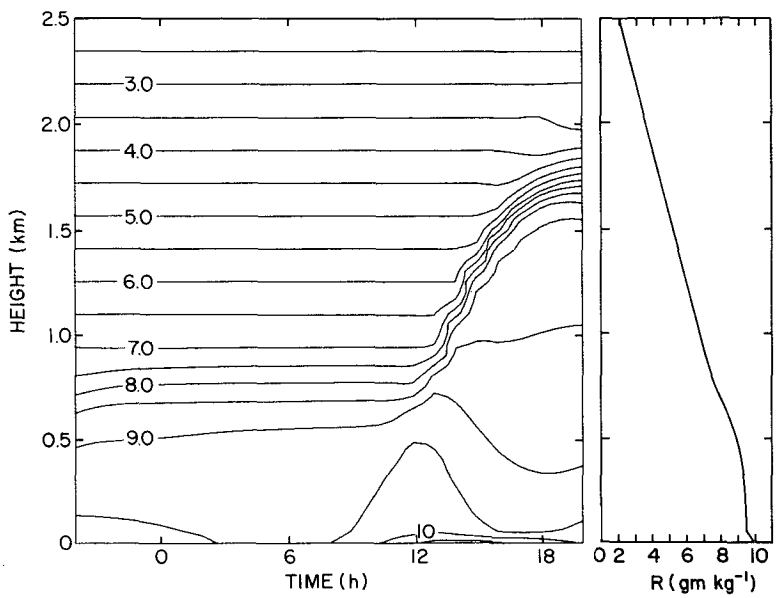

FIG. 3. First 24 h evolution of the specific humidity field (g kg^{-1}). Initial specific humidity distribution at right.

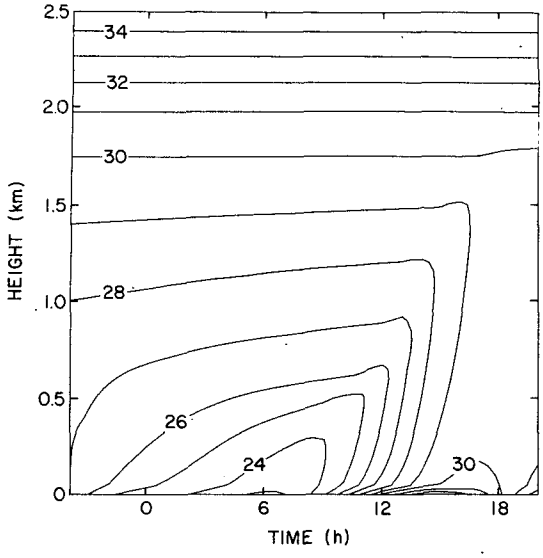

FIG. 4. First 24 h evolution of the virtual potential temperature field (°C).

initial moisture distribution is shown in detail by the curve at the right in Fig. 3. It is assumed that a considerable moisture lapse is present initially above ~0.5 km. This allows a test. Can dry air entrainment and surface evaporation maintain this moisture lapse in the face of turbulent mixing associated with boundary layer growth in the afternoon?

Clearly, the moisture distribution beginning the second 24 h period of integration is considerably different than the initial, strong moisture lapse distribution. Moreover, substantial change is evidenced in the virtual potential temperature field (Fig. 4). Here the development of a nocturnal inversion and a deep, nearly neutral thermal layer in late afternoon are apparent.

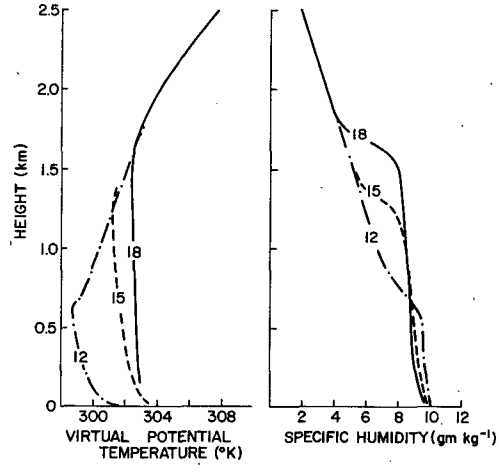

FIG. 5. Vertical moisture and thermal distributions at three selected times of day 1.

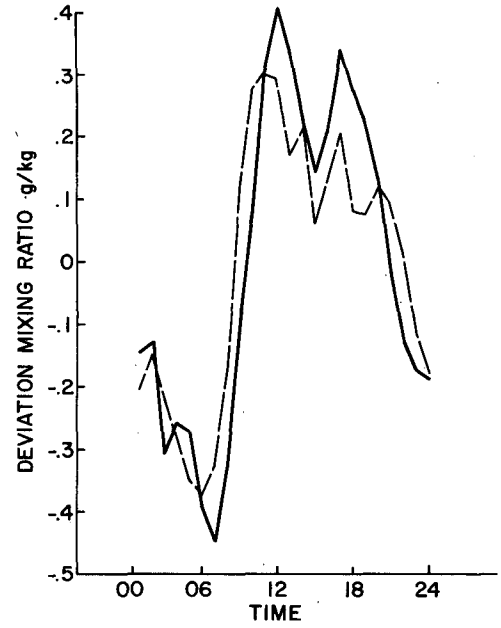

FIG. 6a. Mean diurnal deviation of mixing ratio from daily average. Taken from tower data of Schaefer (1976). (Dashed 89.5 m, solid 443.8 m.)

During the afternoon, above the surface boundary layer, convective development of a well-mixed moist layer is evident (Fig. 3), and reaches a height of ~1500 m by late afternoon. A moisture lapse of only ~0.75 g kg^{-1} km^{-1} exists within this layer at 1800 LT (Fig. 5). Since turbulence is negligible in the high altitude stable region, there is no convective redistribution of moisture,

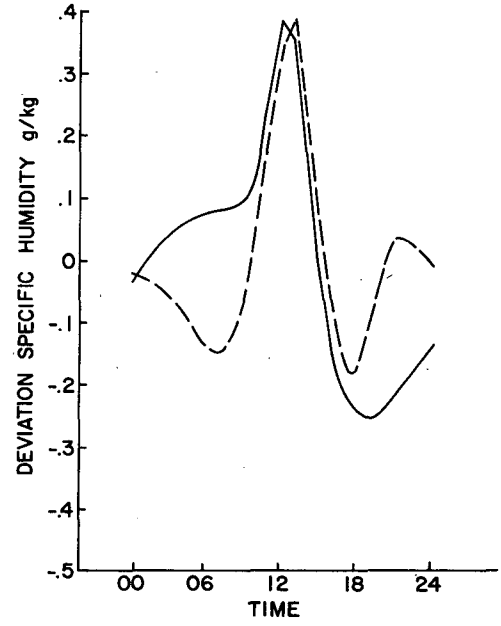

FIG. 6b. Calculated deviation of specific humidity from daily average. (Dashed 100 m, solid 450 m.)

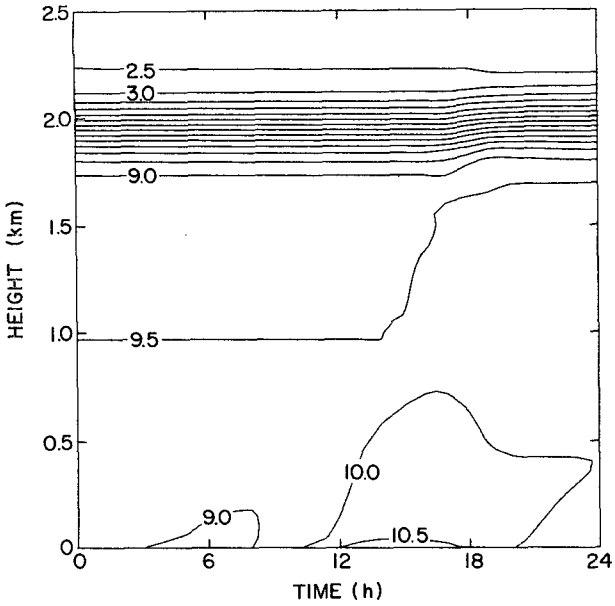

FIG. 7. Specific humidity field (g kg^{-1}) for day four.

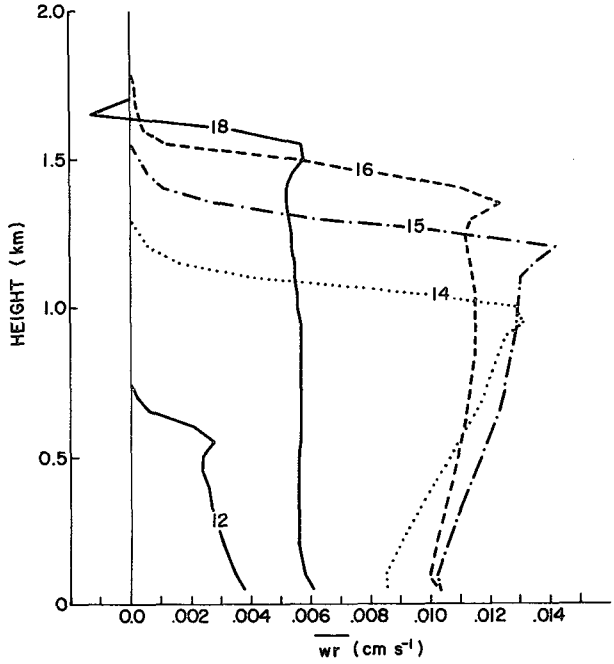

FIG. 8. Moisture flux distributions at various times of day 1.

and the moisture lapse remains at its initial value of $\sim$3.1 g kg^{-1} km^{-1}. Profiles such as those in Fig. 5 also present an interesting problem. How are we to properly define the thermal and moist boundary layer depths? For the heated, growing PBL the top of the thermal boundary layer is generally defined as the height Z_i, where the virtual heat flux $\overline{w\theta_v}$ is most negative. When heat flux information is unavailable such as with radiosonde profiles then the center of the capping inversion in the θ_v profile normally is taken to give Z_i (e.g., Melgarejo and Deardorff, 1974). These two methods of locating Z_i yield essentially identical results in this model and in Deardorff's (1974a, Fig. 1a) three-dimensional PBL model.

Specification of the moist boundary layer depth Z_m is somewhat more difficult. Perhaps the most direct approach is based upon the specific humidity profiles such as those in Fig. 5. These R profiles exhibit a transition layer from a "shoulder" at which R initially deviates from its mixed layer profile to a height at which air totally unmodified by boundary layer processes is encountered.[1] It is only because we are dealing with ensemble mean values that this transition layer has a smooth appearance since air having significantly different temperature and moisture characteristics is intruding and mixing within this region. In line with the Willis and Deardorff (1974) definition of Z_i as the average height of the wavy transition interface in their laboratory tank model, Z_m may be located at the center of the transition layer in the R profile.

Then our results show that $Z_m = Z_i$. This is also true of the Deardorff model. However, it should be noted that the height at which the upward moisture flux $\overline{wr}$ reaches a maximum in the heated PBL corresponds more closely to the height of the shoulder in the R profile than to the center of the transition layer. This distinction becomes important later when we evaluate

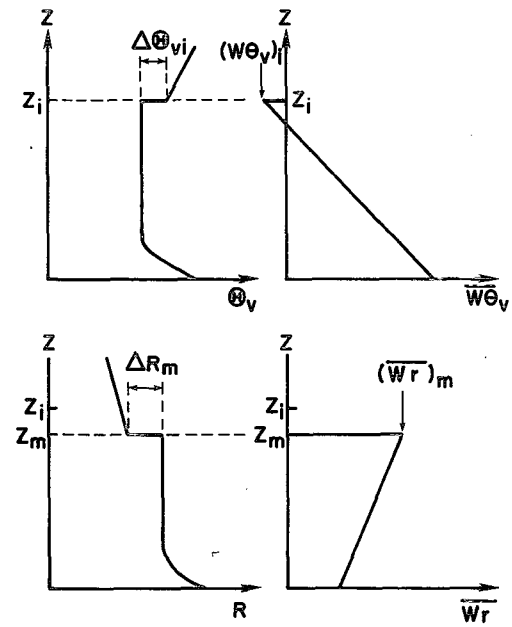

FIG. 9. Virtual potential temperature and heat flux profiles used in simple, analytic "jump" models (a) and specific humidity and moisture flux profiles for analytic computations (b).

[1] As noted by a reviewer, it is reassuring to see that this model predicts a very reasonable thickness for the transition layer on the order of 20% of Z_i.

TABLE 1. Evaluation of Eq. (2) using results from the numerical model.

Hour	Z_m (m)	$-\Delta R_m$	$(\overline{wr})_m$ (cm s^{-1})	$(\overline{wr})_{am}$ (cm s^{-1})	$\frac{dZ_m}{dt}$	$\frac{\Delta R_m}{(-\overline{wr})_m}$
14	950	0.0025	0.0130	0.0131		1.21
15	1200	0.0028	0.0134	0.0142		1.17
16	1350	0.0032	0.0116	0.0123		0.97
17	1450	0.0035	0.0085	0.0092		1.12
18	1550	0.0038	0.0053	0.0057		1.0

analytic methods of calculating the moist layer's growth rate.

FIG. 6a shows the mean diurnal deviation of mixing ratio from the daily average at two selected heights from Schaefer's (1976) tower data. Here the characteristic features (principal minimum in early morning and midafternoon secondary minimum) are apparent. In Fig. 6b specific humidity deviations from the mean are shown for day 1 of numerical integration at grid points having heights nearest those of the tower data. The midafternoon minimum has become the principal minimum. Thus, although the *surface* specific humidity is increasing during the period 1200 to 1500 LT (Fig. 1), at heights of 100 and 450 m the specific humidity rapidly is decreasing during the time period. At these levels there is a moisture flux divergence with the turbulent entrainment of dryer air from above rather than moisture supplied from below dominating the process. In late afternoon (or early evening) the turbulence intensity diminishes sharply so that the convective drying process becomes ineffective as again at these levels humidity increases in response to upward moisture flux from below. No attempt was made to simulate precisely Schaefer's results which are the composite of a large number of daily measurements. Rather, simply certain broad features in the daily humidity curves are examined.

As integration proceeds into subsequent days, the moist layer becomes more well-mixed and the midafternoon specific humidity profile changes significantly. Dry air entrainment from above is much less effective in this well-mixed environment and the surface moisture flux to a large extent controls the specific humidity distribution. After four days the midafternoon specific humidity minimum at low levels has been replaced by a maximum (Fig. 7) closely coincident with the surface moisture maximum. Thus, if we compile composite profiles of daily specific humidity variation, the results would differ significantly from the day-1 profile (Fig. 6b). However, we could not hope to duplicate accurately the experimental results (Fig. 6a) since the model does not deal with advective effects.

In this experiment the choice of surface specific humidity used (Fig. 1) leads to a net moisture transfer to the atmosphere during the period of one day. Strong afternoon turbulence leads to large upward moisture fluxes, while at night the downward turbulent flux is much weaker. Of course, such a net upward moisture flux from the surface is not unrealistic since the surface generally acts as a moisture source to the atmosphere, with precipitation and condensation at the surface (e.g., dew formation) acting as the principal sinks. Although no precipitation mechanism is parameterized in the model, in the next section the effects of dew formation are simulated to some extent.

The moisture flux distribution at various times during day 1 of the integration is shown in Fig. 8. Whereas the afternoon heat flux monotonically decreases with height from its surface value, the moisture flux actually can reach a maximum at high altitude. This maximum results from dry air entrainment at the top of the mixed layer accompanied by the upward transport of more moist air, yielding a significant upward moisture flux. In the days following when the boundary layer is not growing into such a dry environment as was initially present, the moisture flux curves decreases in magnitude and become smoother in character. Then the curves resemble those Deardorff (1974a) presented with his simulation of Wangara data.

There has been considerable analytic investigation of the growth rate dZ_i/dt of the thermal boundary layer. For simplicity, virtual potential temperature and heat flux profiles in these analytic models generally are specified to have the form shown in Fig. 9a. Such studies predict the rate of rise of Z_i to be

$$\frac{dZ_i}{dt} - W_i = -\frac{\overline{(w\theta_v)_i}}{\Delta\theta_{vi}}, \tag{1}$$

where W_i (zero in our model) is the mean value of the vertical motion at $Z=Z_i$, $-\overline{(w\theta_v)_i}$ the virtual heat flux at Z_i and $\Delta\theta_{vi}$ the virtual potential temperature jump at Z_i. If we model the specific humidity and moisture flux profiles as shown in Fig. 9b, an expression for the moist layer's growth rate dZ_m/dt can be derived in a manner similar to that used by Lilly (1968) in obtaining Eq. (1). Such a derivation yields

$$\frac{dZ_m}{dt} = -\frac{(\overline{wr})_m}{\Delta R_m}, \tag{2}$$

where $\Delta R_m = R(Z_m+\epsilon) - R(Z_m-\epsilon)$ and ϵ is a small positive depth.

Results from the numerical model may be used to make calculations with Eq. (2). Note that in Fig. 9b, Z_m is taken to be distinct from Z_i. Thus, in this analytic "jump" model we are taking advantage of our observation that in the growing PBL the peaks in the $\overline{wr}$ profiles (Fig. 8) occur somewhat below Z_i. As noted previously, these peaks in $\overline{wr}$ coincide with the location of the shoulder in the R profile. In the absence of moisture flux profile information, the shoulder in R may be used to locate Z_m for jump model calculations.

First the actual moisture profiles (Fig. 5) are approximated with profiles consisting of straight line segments fitted to the actual profiles at heights well above and below Z_m. Then these line segments are extended to Z_m. This typically results in a specific humidity jump ΔR_m at Z_m. Similarly, well within the mixed layer, line segments are fitted to the profiles of $\overline{wr}$ and extended to Z_m to give values of $(\overline{wr})_m$. Thus, evaluation of the quantities appearing in Eq. (2) is possible.

Table 1, showing the result of such calculations, includes the quantity $(dZ_m/dt)\Delta R_m/(-\overline{wr})_m$ which should equal unity according to Eq. (2). Also presented in Table 1 are the actual values $(\overline{wr})_{a_m}$ of the moisture flux at Z_m taken directly from the numerical results. Deardorff (1974a) made similar computations to test the validity of jump models by utilizing the results of his PBL model. Deardorff evaluated these moisture related quantities at height Z_i by the expression

$$(\overline{wr})_i = -\left(\frac{dZ_i}{dt}\right)\Delta R_i. \tag{3}$$

For comparison, extending our fitted line segments to the height Z_i allows evaluation of quantities in Eq. (3). Table 2 presents the results of such an approach for the model. Here $(\overline{wr})_{a_i}$ represents the actual moisture flux at Z_i taken directly from the numerical model. Examining Tables 1 and 2 reveals that Eq. (2) is more nearly satisfied (e.g., the ratio of terms is more nearly unity) than is Eq. (3). Further, it is apparent that calculations using Eq. (2) give good estimates of the actual flux at height Z_m. On the other hand, use of Eq. (3) gives considerable overestimates of the moisture flux at Z_i. This results from the rapid decrease in upward moisture flux between Z_m and Z_i. Hence, it is clear why Deardorff (1974a) found actual values of the moisture flux from his PBL model as much as 40% less than values calculated from Eq. (3). Therefore, for purposes of calculations with analytic jump models it is convenient to treat the top of the moist boundary layer as being located at $(\overline{wr})_{\max}$. This is the point of the present discussion and not an attempt to supplant the more standard definition which locates Z_m at the center of the transition layer in the R profile.

TABLE 2. Evaluation of Eq. (3) using results from the numerical model.

Hour	Z_i (m)	$-\Delta R_i$	$(\overline{wr})_i$ (cm s^{-1})	$(\overline{wr})_{a_i}$ (cm s^{-1})	$\frac{dZ_i}{dt}\frac{\Delta R_i}{(-\overline{wr})_i}$
14	1100	0.0029	0.0138	0.0041	1.44
15	1350	0.0034	0.0137	0.0030	1.40
16	1500	0.0036	0.0116	0.0055	1.09
17	1600	0.0037	0.0085	0.0039	0.61
18	1600	0.0039	0.0053	0.0035	1.0

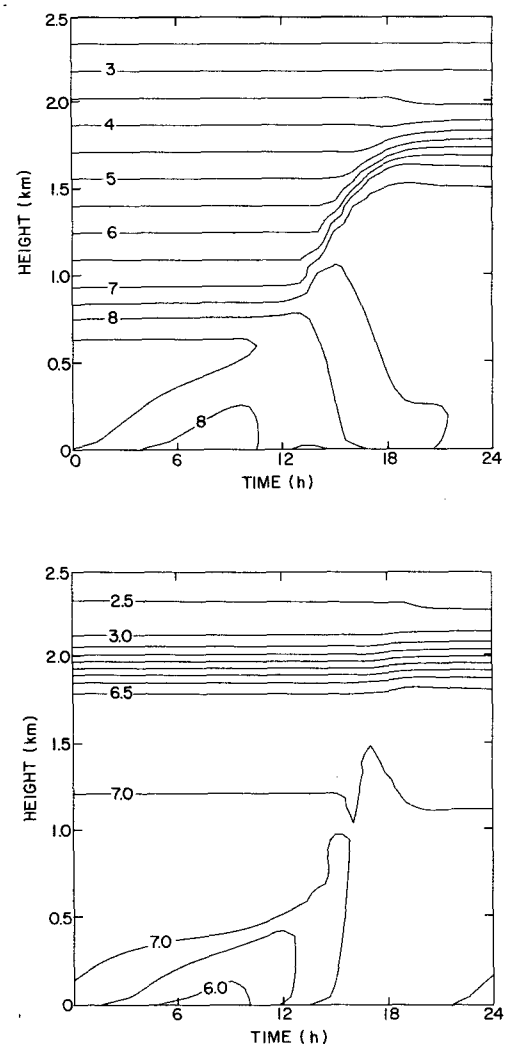

FIG. 10. Specific humidity field (g kg^{-1}) for day 1 of case with surface moisture flux specified to oscillate diurnally (a), and day 4 (b).

b. *Specified surface moisture flux*

Now to investigate briefly several experiments in which the surface moisture flux $(-\overline{wr})_s$ is specified rather than the surface specific humidity R_s. This is the only boundary condition altered from the previous case. In the first experiment, the curve shown in Fig. 1 is used for surface moisture flux instead of specific humidity as in the previous section. This curve gives a near zero net flux over a 24 h period and the temporal spacing between minimum and maximum (9 h) generally is more realistic than that of a simple sinusoidal wave (12 h). The moisture wave scale is determined by an upward flux maximum of 1.3×10^{-3} cm s^{-1} at 1500 m and a downward flux extremum of 8.7×10^{-4} cm s^{-1} at 0600 LT.

The specific humidity configurations during days 1 and 4 of this experiment are displayed in Fig. 10.

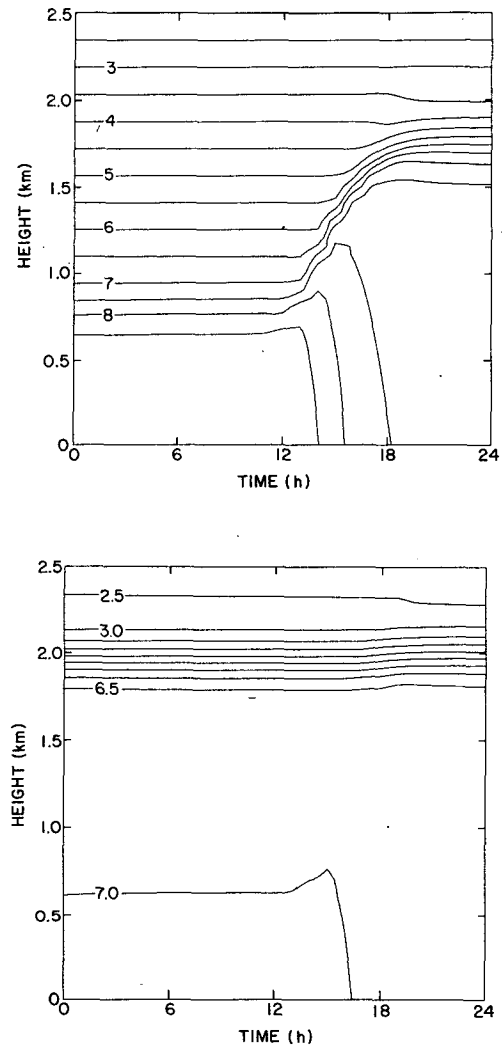

FIG. 11. As in Fig. 10 except no surface moisture flux.

Figs. 3 and 10a compared at high levels show similar moisture structure in the two experiments and results which are relatively unaffected by the nature of the surface moisture boundary condition. However, near the surface (Fig. 10) a well-developed morning moisture inversion exists in associated with the downward nocturnal moisture flux at the surface. Such a low-level moisture inversion is a typical feature under conditions of dew formation (Moses *et al.*, 1968). Since the surface temperature is specified rather than calculated from energy budget considerations, there is no attempt to account for the thermodynamic effects of latent heat release during the dew formation process.

Also computed are the temporal variations in the moisture column abundance during each of our experiments. Midafternoon low-level minima in moisture content are associated with near maxima in the integrated column abundance of water vapor. This occurs as the moisture is mixed through deeper layers during the rapid midafternoon growth of the PBL. This vertical redistribution of the water vapor content can produce an increase in the atmospheric static stability (as measured by the virtual potential temperature distribution) and thereby adversely affected the likelihood of precipitation.

The diurnal behavior of the moisture configuration above a dry, desert-like surface is the objective of the final numerical experiment. Here the surface moisture flux is set to zero, while the initial and boundary conditions are similar with those of previous experiments. Fig. 11 shows the moist layer evolution for days 1 and 4. During the first day of integration, the mixed layer shows a monotonic decrease in specific humidity, particularly in the afternoon. The low-level moisture is mixed through a deep layer in the afternoon with no compensating surface moisture influx. Under these conditions, once a deep well-mixed moist layer is established its stratification remains virtually unchanged throughout a diurnal cycle. There is no moisture flux at the surface to alter the stratification and the flux through the capping inversion is weak because the well-mixed layer has been extended throughout the depth penetrated by the afternoon turbulence.

4. Summary

The structure and temporal behavior of the moist boundary layer is examined by means of a higher order turbulence closure model similar to Mellor (1973) and Mellor and Yamada (1974). Both the diurnal behavior of the moist layer as a whole and numerous micrometeorological measurements are simulated over varying geographic regions. Strong nocturnal moisture inversions are found associated with substantial downward surface moisture fluxes (such as occur when there is dew formation). In a case having a moist surface, the midafternoon maximum in surface evaporation and turbulent transfer of moisture to higher levels act as competing processes in determining low-level moisture content. When moisture transfer to higher levels dominates, a relative minimum occurs in midafternoon specific humidity at low levels. Coupled with the evaporation minimum associated with the surface temperature minimum, the daily specific humidity profile at low levels shows the frequency observed double wave structure.

Further, results indicate that entrainment of dry air associated with a boundary layer growing rapidly into an overlying dry environment is insufficient to create or to maintain a strong vertical moisture gradient. If true, this points to the vertical variations of horizontal moisture advection as the most likely mechanism to produce the coexisting strong moisture lapses and thermally well mixed boundary layers discussed by Mahrt (1976). Mahrt presents results which tend to corroborate this point, but notes that an unambiguous conclusion cannot be reached from his analysis due to

possible enhanced mixing or entrainment associated with advection of temperature or mixed layer depth. Clearly, I cannot hope to resolve this latter point with the current one-dimensional model.

Model results show that the usual placement of the mean mixed layer top Z_m at the center of the transition layer in the specific humidity profile results in $Z_m = Z_i$. Analytical methods of calculating the growth rate of the moist boundary layer along the lines indicated by Lilly (1968) are compared with results from the numerical model. For such computations, it is found profitable to use an alternative definition which locates Z_m at the height where $\overline{wr}$ is a maximum. In the heated PBL this height closely coincides with the shoulder in the R profile and is generally somewhat lower (typically $\sim$100 m) than Z_i. Often there is a sharp decrease in moisture flux above $(\overline{wr})_{\max}$ and one can substantially overestimate the moisture flux at Z_i with an analytic method which ignores this moisture flux decrease.

The ability of the Mellor and Yamada higher-order turbulence closure model to provide realistic simulation of the PBL is impressive. The diurnal variation of many quantities which were calculated (but not explored in this paper, e.g., wind and temperature fields, turbulent kinetic energy and stress distributions, etc.) were found to be in good agreement with the Mellor and Yamada (1974) dry PBL model. Thus, the results also represent an independent confirmation of their model (excepting the computational difficulties discussed in the Appendix). Finally, the Level 3 version of their model used herein sacrifices little in predictive accuracy and provides a considerable computational savings over the Level 4 model in which differential equations are solved for all turbulent moments.

Acknowledgments. The author is grateful to Dr. J. Schaefer for many valuable discussions. Dr. Schaefer also kindly furnished Fig. 6a. Thanks also are extended to Drs. C. Doswell, L. Mahrt and T. Yamada for their helpful comments on this manuscript and to Mrs. H. Ardrey for editorial assistance. The author conducted this research as a National Research Council resident research associate.

APPENDIX

Finite-Difference Alogrithm and Computational Stability

Yamada and Mellor (1975) have shown that all of the differential equations solved in their Level 3 model can be reduced to the form[2]

$$\frac{\partial \phi}{\partial t} = \frac{\partial}{\partial Z}\left(P_1 \frac{\partial \phi}{\partial Z}\right) - P_3\phi + P_4, \tag{A1}$$

where ϕ, P_1, P_3 and P_4 are identified in their Table 1. The finite-difference expression for (A1) utilized by Yamada and Mellor is

$$\phi_j^{n+1} - \phi_j^n = \frac{\delta t}{2(\delta Z)^2}\left[(P_{1_{j+1}}^n + P_{1_j}^n)\phi_{j+1}^{n+1} - (P_{1_{j+1}}^n + 2P_{1_j}^n + P_{1_{j-1}}^n)\phi_j^{n+1} + (P_{1_j}^n + P_{1_{j-1}}^n)\phi_{j-1}^{n+1}\right] - \delta t(P_{3_j}^n \phi_j^{n+1} - P_{4_j}^n), \tag{A2}$$

where for simplicity of discussion uniformity of grid spacing is assumed. Here j and n label the jth grid point from the surface at the nth time step. The vertical grid spacing is δZ and the time step is δt. In particular note that the variable ϕ on the right of (A2) is evaluated at the $(n+1)$th time step, while the P values are evaluated at time step n.

By a linear stability analysis (treating P_1 and P_3 as constants and setting P_4 to zero) one can show that (A2) is unconditionally stable provided P_3 is not negative.

However, in the equations which are actually being integrated P_4 may be a direct function of the variable ϕ. For instance, in the differential equation for $\overline{\theta_v^2}$ we have

$$P_4 \equiv -\overline{w\theta_v}\frac{\partial \theta_v}{\partial Z}. \tag{A3}$$

Substituting for $-\overline{w\theta_v}$ from Eqs. (21) and (23a) of Yamada and Mellor shows that the expression for P_4 contains the term $\overline{\theta_v^2}$ explicitly. Thus, in effect, $\overline{\theta_v^2}$ is evaluated at time step n in the term P_4, while at time step $(n+1)$ in the other terms on the right-hand side of (A2). A similar situation arises in the equation for $\overline{r^2}$.

This dependence of P_4 upon ϕ created no difficulty in the numerical integration via the scheme outlined in (A2) *except* in regions of large stability. Under highly stable conditions situations were occasionally encountered in which the P_4 term explicitly involving ϕ was the dominant term in (A2). (Although generally all of the terms were of small magnitude under these conditions.) In such a situation (A2), in effect, reduces to

$$\phi_j^{n+1} - \phi_j^n \approx -C\delta t \phi_j^n, \tag{A4}$$

where $P_4 = -C\phi$ with C being treated as a positive constant for simplicity. Effectively the differential equation reduces to

$$\frac{\partial \phi}{\partial t} \approx -C\phi, \tag{A5}$$

with (A4) being its finite-difference analog. Rewriting (A4) as

$$\phi_j^{n+1} \approx (1 - C\delta t)\phi_j^n, \tag{A6}$$

[2] Yamada and Mellor also have a P_2 term involving the vertical advection of potential temperature. This term is zero here since we have $W = 0$.

it is apparent that if $C\delta t>1$, (A6) gives an oscillating in sign, multiplicatively growing series when finding new values of ϕ by time marching. Thus, when $C\delta t>1$, the simple finite-difference expression (A4) is a startling failure as an analog to (A5) whose analytic solution obviously is an exponential decay of ϕ with time.

To avoid this difficulty I write out the P_4 terms explicitly and transfer those portions of P_4 containing ϕ into the $P_3^n\phi_j^{n+1}$ term in (A2).[3] Now when the type of situation which had previously presented difficulty is encountered, the finite-difference scheme reduces to

$$\phi_j^{n+1}-\phi_j^n\approx C\delta t\phi_j^{n+1} \tag{A7}$$

or upon rearranging,

$$\phi_j^{n+1}\approx\phi_j^n/(1+C\delta t). \tag{A8}$$

This represents an acceptable, albeit not particularly accurate, analog to (A5). It possesses the feature being sought, namely, stability even when $C\delta t>1$. High accuracy is not required under these highly stable conditions since the tendencies are very small.

[3] Thus, P_3 and P_4 in the last row of Table 1 of Yamada and Mellor's paper should be

$$q/\Lambda_2+(\gamma_c/\overline{\theta^2})\frac{\partial\theta_v}{\partial z} \quad \text{and} \quad K_H'\left(\frac{\partial\theta_v}{\partial z}\right)^2,$$

respectively.

REFERENCES

Carson, D. J., 1973: The development of a dry inversion-capped convectively unstable boundary layer. *Quart. J. Roy. Meteor. Soc.*, **99**, 450–467.

Clarke, R. H., A. J. Dyer, R. R. Brook, D. G. Reid and A. J. Troup, 1971: The Wangara experiment: Boundary layer data. Tech. Pap. No. 19, Div. Meteor. Phys., CSIRO, Aspendale, Australia, 340 pp.

Deardorff, J. W., 1974a: Three-dimensional numerical study of the height and mean structure of a heated planetary boundary layer. *Bound.-Layer Meteor.*, **7**, 81–106.

——, 1974b: Three-dimensional numerical study of turbulence in an entraining mixed layer. *Bound.-Layer Meteor.*, **7**, 199–226.

Donaldson, C. duP., 1973: Construction of a dynamic model of the production of atmospheric turbulence and the dispersal of atmospheric pollutants. *Workshop on Micrometeorology*, Amer. Meteor. Soc., 313–392.

Geiger, R., 1965: *The Climate Near the Ground*. Harvard University Press, 494 pp.

Kuo, H. L., 1968: The thermal interaction between the atmosphere and the earth and propagation of diurnal temperature waves. *J. Atmos. Sci.*, **25**, 682–706.

Launder, B. E., G. J. Reece and W. Rodi, 1975: Progress in the development of a Reynolds-stress turbulence closure. *J. Fluid Mech.*, **68**, 537–566.

Lewellen, W. S., M. Teske and C. duP. Donaldson, 1973: Application of turbulence model equations to axisymmetric wakes. *AIAA J.*, **12**, 620–625.

Lilly, D. K., 1968: Models of cloud-topped mixed layers under a strong inversion. *Quart. J. Roy. Meteor. Soc.*, **94**, 292–309.

Lumley, J. L. and B. Khajeh-Nouri, 1974: Computational modeling of turbulent transport. *Advances in Geophysics*, Vol. 18A, Academic Press, 169–192.

Mahrt, L., 1976: Mixed layer moisture structure. *Mon. Wea. Rev.*, **104**, 1403–1407.

——, and D. H. Lenschow, 1976: Growth dynamics of the convectively mixed layer. *J. Atmos. Sci.*, **33**, 41–51.

Melgarejo, J. W., and J. W. Deardorff, 1974: Stability functions for the boundary-layer resistance laws based upon observed boundary-layer heights. *J. Atmos. Sci.*, **31**, 1324–1333.

Mellor, G. L., 1973: Analytic prediction of the properties of stratified planetary surface layers. *J. Atmos. Sci.*, **30**, 1061–1069.

——, and T. Yamada, 1974: A hierachy of turbulence closure models for planetary boundary layers. *J. Atmos. Sci.*, **31**, 1791–1806.

Moses, H., W. C. Ashby and M. A. Bogner, 1968: Dewpoint temperature inversions. *J. Appl. Meteor.*, **7**, 206–216.

Schaefer, J. T., 1976: Moisture features of the convective boundary layer in Oklahoma. *Quart. J. Roy. Meteor. Soc.*, **102**, 447–451.

Stull, R. B., 1973: Inversion rise model based on penetrative convection. *J. Atmos. Sci.*, **30**, 1092–1099.

Tennekes, H., 1973: A model for the dynamics of the inversion above a convective boundary layer. *J. Atmos. Sci.*, **30**, 558–567.

Willis, G. E., and J. W. Deardorff, 1974: A laboratory model of the unstable planetary boundary layer. *J. Atmos. Sci.*, **31**, 1297–1307.

Yamada, T. and G. Mellor, 1975: A simulation of the Wangara atmospheric boundary layer data. *J. Atmos. Sci.*, **32**, 2309–2329.